IEEE Access
Multidisciplinary | Rapid Review | Open Access Journal

Received 15 November 2022, accepted 8 December 2022, date of publication 15 December 2022,
date of current version 20 December 2022.

Digital Object Identifier 10.1109/ACCESS.2022.3229597

RESEARCH ARTICLE

Design, Modeling and Hardware Implementation of Regenerative Braking for Electric Two-Wheelers for Hilly Roads

TAKO NAMA, (Student Member, IEEE), PROSENJIT MONDAL, PRAVEEN TRIPATHY, (Member, IEEE), RAVINDRANATH ADDA, (Member, IEEE), AND ANUP KUMAR GOGOI
IIT Guwahati, Guwahati, Assam 781039, India
Corresponding author: Tako Nama (tako.nama@iitg.ac.in)

ABSTRACT The electric vehicles which operate in hilly region gain potential energy while moving uphill. Some of this energy can be recuperated to charge the battery while the vehicle moves downhill by using regenerative braking. The speed of the electric vehicle while descending the slope of hilly roads is often low to ensure the safety of the passenger, hence requiring regenerative braking at low speed. Braking at low speed is quite challenging due to the low level of back electromotive force (EMF) during regenerative braking. This paper presents a modular regenerative braking circuit for electric scooters operating at low speeds. The proposed modular regenerative braking circuit's configuration, operation, and control scheme are explained in the paper. Here using the state-space averaging technique, the small-signal modeling of the braking circuit was done, and a Type-II current controller was designed to track the braking current reference. The proposed configuration also suggests fast switching between the motoring and regenerative modes by enabling or disabling the gate pulses to the inverter or DC/DC boost converter. This removes the need for a separate switch in the power circuit, hence increasing reliability and reducing cost. The operation of the proposed regenerative braking circuit, along with the overall motor drive-train of the vehicle, was simulated in MATLAB/Simulink. Its hardware implementation was conducted on a scaled-down laboratory test set-up. The simulation and experimental results verify the working of the proposed regenerative braking circuit and the effectiveness of the proposed control scheme.

INDEX TERMS Modular regenerative braking, electric scooters, DC/DC converter, Type-II compensator, hilly roads.

I. INTRODUCTION

Today Electric Vehicles (EVs) are one of the key players in the clean and sustainable technology sector. A decade ago, a paradigm shift in the transportation system from transportation 1.0 to transportation 2.0 was postulated in [1]. Wherein transportation 1.0 referred to a conventional fossil fuel-dependent transportation system, and transportation 2.0 referred to the then-upcoming new generation of electrified vehicles. From 2020 to 2021 there was a 108% boost in global electric car sales as reported by International Energy Agency (IEA) [2]. Nearly 6.6 million registered electric cars are on the road. This number includes passenger vehicles, light trucks, and light commercial vehicles. The impressive sale growth of EVs indicates the dawn of transportation 2.0, and they are here to stay.

Although EVs have many benefits over internal combustion (ICE) vehicles, like them being more efficient, more reliable, safer, smarter, and, most importantly, environmentally friendly [1]. However, their range is still a major challenge. The range of an EV is the distance covered when fully charged [3]. The battery (energy source) that powers

The associate editor coordinating the review of this manuscript and approving it for publication was Amin Mahmoudi.

the EVs has a lower energy density than gasoline fuel used in ICE vehicles. The range of the EVs further goes down when operating on the hilly region roads. Due to the road gradient, the battery has to supply more power to overcome the tractive resistive force on an inclined road than on a plain road for a given distance to cover at the same speed [4], [5]. If we only consider the battery power consumption, *i.e.* kWh per hour, the hilly region roads become unfriendly to EVs [6].

In the past and the present, many studies have been done to improve the EV range. In literature, different methods have been reported to increase EV's range and fuel economy. The power train of an EV classically consists of an energy source, an electric circuit (power electronics), electronic control unit (ECU) and an electric motor. Now the contributions to tackle the range extension problem are being made from all the different parts of the EV drive line. A comprehensive topological overview of power trains for battery-powered vehicles with range extenders is given in [7] and [8], and some critical technologies for electric vehicles are discussed in [9]. Since battery is the primary energy source, special attention has been given to battery technology to make it a good lasting source. Choosing the correct type of energy source can give longer range, for example, Li-Ion batteries over lead acid batteries. Li-Ion batteries have been found to have a high energy density and longer lifespan compared to their other counterparts [10], [11]. Work at the nascent stage combines fuel cells (with even higher energy density and quicker refill time than a battery) with source batteries to make a longer-lasting energy source [12]. EV range extension is also achieved by system-level modelling of an efficient cell balancing circuit of the battery packs [13]. Also, maintaining the battery to operate at an optimum temperature has improved the battery's life span and increased in EV range [14]. Then, opting for newer, highly efficient designed motors like SRM, PMSM, and BLDC over DC motors shows better performance and less fuel is consumed [15], [16]. In [17], the design of an energy-optimal control method to improve the motor drive system's efficiency and extend the driving range of electric vehicles is studied.

So far, the methods discussed above for the range extension were to reduce and optimise power consumption or increase the capacity of the source battery. The other way to extend the EV range is to recover the energy already spent. That is the regeneration way. For example, incorporating a regenerative braking system (RBS) over conventional friction braking during the retardation period of the wheels also has been reported to increase the driving range [18], [19]. It is "regenerative" braking because it converts the moving wheel's kinetic energy (mechanical energy) into electrical energy and charges the source battery during the braking period of the vehicle. In an ICE vehicle, this same energy would have been absorbed in the form of heat in friction-based braking. Studies show a good RBS design enables the EV to increase its driving range by up to 16% to 25% [20], [21]. An RBS consists of the braking device (*i.e.*, the interface between the human and

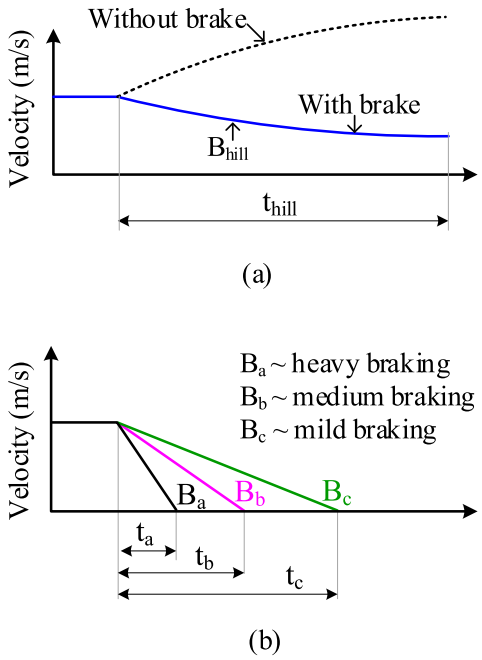

FIGURE 1. Types of braking force application; (a) braking force applied for a longer duration to descend the vehicle at low speed on the hill slope (b) braking force applied for a short period to quickly stop the vehicle, as seen in urban drives.

the vehicle which converts the braking force into an electrical quantity), the regenerative braking circuit, the energy storage device, and the electronic control unit (ECU). The work done in this paper present a regenerative braking circuit which falls within the subset of the regenerative braking system.

The regenerative braking circuit in the RBS can be realised by using the existing inverter of the EV powertrain or by using additional components. Based on this factor, the regenerative braking circuit topology can be classified into two types, i.e. Type-I and Type-II; Type-I is for those using the same inverter circuit, and Type-II is for those using additional circuits or components. A comprehensive literature review on the current and previous state of braking circuit topologies is given in Table 1, which is also supported by its simple block diagram representation in Fig. 2. From the literature review, it is inferred that designing a regenerative braking circuit is a case of "no one size fits all," meaning based on the factors like power handling, vehicle size and terrain application, the designs call for a unique braking circuit. For example, when designing an electric braking circuit for a railed vehicle like urban rail transit trains, where braking power density is high. In such a case, it seems more appropriate to use an additional DC/DC converter to charge a stationary supercapacitor energy storage system [22].

Likewise, for road vehicles, the nature of braking action on a plain road, as mostly seen in urban city drives, is quite different from that of hilly road drives in hill stations. On hilly roads, the brake is mainly applied to descend at a comfortable low-speed and prevent the vehicle from over-speeding as illustrated in Fig. 1 (a). Comparing Figs. 1 (a) and (b), it is

TABLE 1. Comprehensive review on regenerative braking circuit topologies used in electric vehicles.

Reference	Type	Remarks
M.J. Yang, et. al [21], M. U. Deepa, et. al [23], T. Soylu, et. al [24],	Type-I	• The Type-I category employs the same inverter circuit of the EV power train as the regenerative braking circuit, as shown in Fig. 2 (a). • This topology only modify the inverter's switching pattern during the braking phase to regulate the inverse torque and ensure that the braking energy is sent back to the battery. • The benefit of using the same motor drive inverter circuit as a regenerative braking circuit is to minimize the number of power devices, hence, is more economical. • The limiting factor of this type is that it is not suitable for low speed and heavy duty vehicles. The switch in the inverter needs to supply more power to the propulsion motor, its switching frequency is low compared to the typical switching frequency used in the DC/DC converter needed to boost very low voltage.
Heydari, et. al [25], [26]	Type-I	• Since this (Type-I) topology is not suitable for the low-speed application, Heydari *et al.* proposed a boundary in the braking force distribution where the combination of regenerative and friction braking is carried out to maximise energy recovered through the regenerative braking process which is defined using the performance map of the traction motor (TM) and its controller.
A. J. Godfrey, et. al [27]	Type-I	• Godfrey *et al.*, proposed new electric braking based on the stopping time and energy regeneration; here, a combination of regenerative and plugging for braking is presented using the same inverter drive circuit for low speed application.
X. Nian, et. al [28], X. Zhang, et. al [29], G. Xu, et. al [30]	Type-I	• In these three papers the optimization of regenerative braking is studied. Fuzzy logic control [28] is used to distribute braking force, Tagaki-Sugeno fuzzy model [29] and a knowledge based methodology in a hierarchical control structure [30] is studied for the stability and improvement of the braking performance.
J.W. Dixon, et. al [31], J. Dixon, et. al [32], M. Ortuzar, et. al [33]	Type-II	• The Type-II category uses additional circuit like DC/DC converter or components as regenerative braking circuit. This category comes with different variant as explained below. • In [31]–[33] a buck-boost converter is employed as regenerative braking circuit. The block representation is shown in Fig. 2 (b). During the braking period, the buck converter is activated, and the recovered energy during the quick deceleration period is sent to the UC. • The advantage of this topology is that the voltage of the dc-link is relatively constant as the battery is connected to the dc-link, which makes the voltage control loops simple. • This arrangement is suitable for quick acceleration and deceleration periods, not for hilly region braking. It's also important to note that regenerative braking using solely UCs is ineffective on steep downhills because they eventually hit their maximum voltage and become incapable of receiving any more power as pointed out by the authors [32].
J. H. Lee, et. al [34]	Type-II	• Lee *et al.* uses a bidirectional DC/DC converter as a regenerative braking circuit as shown in Fig. 2 (c). Here three half-bridge buck-boost converters are connected in parallel to form the DC/DC converter that is being used during the braking period. During the braking period, the DC/DC converter act like a buck converter and the regenerative energy is sent back to the battery. • The interleaved converter has the benefit of allowing for a reduction in the converter's inductance and capacitance, which are governed by the tolerance range of current and voltage ripple. • The disadvantage of this topology is that the extra three numbers of inductance increase the weight of the overall topology.
K. Suresh, et. al [35]	Type-II	• A multi-port and multi-functional converter for electric vehicle (EV) applications with regenerative charging ability is discussed in [35]. The converter exhibits bidirectional power flow functionality making it suitable for charging the battery during regenerative braking as shown in Fig. 2 (d). During the braking period the DC/DC converter act like a buck converter to charge the battery. • The advantage of this converter is its ability to accommodate energy resources with different voltage and current characteristics. • The limiting factor is that the efficiency of regenerative braking is reduced as a result of the bidirectional DC/DC converter and inverter's power dissipation. Moreover, a buck converter as a braking circuit is unsuitable for low-speed applications.
F. Naseri, et. al [36]	Type-II	• The additional DC/DC converter used in [36] is a buck converter which is used during motoring mode only. During the braking period the inverter circuit, along with the help of an additional switch and diode, acts as regenerative braking, as shown in Fig. 2 (e) . Here, during the regenerative braking process, the dc-link voltage is boosted, and the diode is forward biased. • The advantage is that the regenerative braking energy flows to the supercapacitor or the battery without any power converter thus increasing the efficiency. • The disadvantage of such arrangement is that the voltage of the supercapacitor is always higher than the battery, which puts limitations on system design. Also, the high voltage UC is expensive compared to high power density battery.
S. Jung, et. al [37], Yeo, et. al [38]	Type-II	• In [37], [38], energy recovery is done via an electromagnetic retardation. Here the additional components like switch and capacitor along with the inverter circuit form the braking circuit as shown in Fig. 2 (f). • The advantage of this type of braking circuit is that the technique is based on the resonance of the L-C circuit for AC motors and is suitable for braking operation during very low or high speeds. • The limiting factor of this technique is that it does not apply to other motors which do not have sinusoidal waveforms, for example, BLDC motors with trapezoidal waveforms.

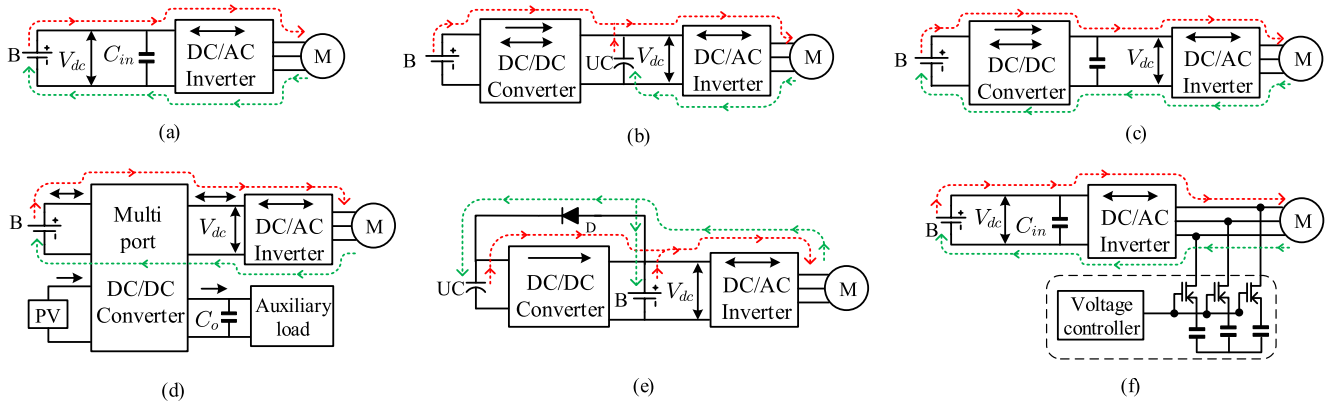

FIGURE 2. State of art of regenerative braking circuit topologies (a) [21], [23], [24], [26], [27], [28], [29], [30], (b) [31], [32], [33] (c) [34] (d) [35] (e) [36] (f) [37], [38].

seen that the braking time required is longer while descending a hill, for such kind of braking; a high power density and a high energy density energy storage are required like Li-Ion [4]. The regenerative braking circuit design and storage device for the hilly road demands to be different from that used in urban plain roads, where it is used to bring the vehicle to a quick stop as shown in Figs. 1 (b).

In braking applications like B_a, B_b, and B_c, as shown in Fig. 1 (b), the kinetic energy needs to be dissipated quickly for the vehicle to stop. The peak power demand of such braking is achieved by using an additional high-power density component like Ultra Capacitors (UC). This combination of an additional energy storage device and the main battery is known as a hybrid energy storage system (HESS). Whenever there is a HESS scheme, they have an additional DC/DC converter to meet the demand. Various HESS configuration and their quantitative comparison are mentioned in [39] and [40] and their different control strategies considering four configurations: fuel cell-battery, battery-UC, fuel cell-UC, and battery-fuel cell-UC are studied in [41]. Numerous UC-based regenerative braking circuits for EVs have been discussed in Table 1 under the Type-II category. However, UCs are expensive, and their control is comparatively complex. In addition, it is also important to note that regenerative braking using UCs solely is ineffective on steep downhills because they eventually hit their maximum voltage and become incapable of receiving any more power [32].

The Type-I category of braking circuit design has less component count and is economically friendly; however, it is not suitable for very low-speed braking and may incur more loss [37]. Efforts have been made to combine this braking circuit with friction braking for very low-speed applications by [25] and many others, as listed in Table 1. Moreover, as the switch in the inverter needs to supply more power to the propulsion motor, its switching frequency is low compared to the typical switching frequency used in the boost converter. Thus limiting voltage gain in regenerative mode. In a hilly region, it is essential to have high voltage gain due to the low value of the back emf generated at low speed. In [37] for

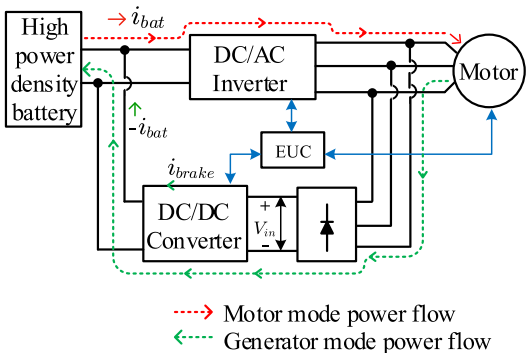

FIGURE 3. Block diagram of the proposed regenerative braking circuit configuration.

low-speed regenerative braking application, Sungchul et al. uses an additional electromagnetic retardation circuit with switch-capacitors connected across the motor windings of PMSM to boost the input voltage seen by the battery terminal based on the resonance of the L-C circuit. However, this technique is based on the resonance of the braking circuit for AC motors. This method is less effective to BLDC motors which have trapezoidal waveforms. Hence, this paper presents a new regenerative braking circuit configuration and its control scheme for low-speed and more extended braking period applications, which can work for all types of three-phase motors, be it either BLDC or PMSM.

The proposed regenerative braking circuit configuration is shown in Fig. 3. It consists of the classical components; a three-phase diode bridge rectifier and DC/DC boost converter. To the best of our knowledge, the proposed configuration (i.e., with DC/DC converter connected in parallel and charging the same battery during regenerative braking) has not been used earlier in a regenerative braking scheme.

The main features of the proposed regenerative braking circuit are:

- The unique feature of the topology is that the regenerative circuit remains connected all the time, and the switching between the motoring and regenerative modes

is done by enabling or disabling the gate pulse to the inverter or the boost converter. Thus, the modes could be switched almost instantly.
- As the switch in the inverter needs to supply more power to the BLDC motor, its switching frequency is low as compared to the typical switching frequency used in the boost converter. Thus present topology supports high switching frequency with improved voltage gain. This helps in developing an effective regenerative system for hilly terrain.
- Here no separate energy source is used thus making the regenerative system more compact and cost-effective.
- Though the system has one additional switch and some passive components but they operate only at the time of the regenerative braking thus increasing the durability and the robustness of the system.
- Due to its modular design, it can be integrated into existing electric scooter which uses mechanical braking with minor modifications.

The other contributions of the paper are designing the current controller for the proposed regenerative braking circuit and experimentally implementing it on a motor drive-train in a scaled-down laboratory test set-up.

The remaining paper is organized as follows; Section II gives the system background and explains the working of the proposed system. Here the mathematical modeling of all the fundamental building blocks of the regenerative braking system and its controller design is presented. Then in Section III, the performance analysis of the proposed braking circuit with simulation results is given. Section IV presents the experimental results and their explanation. Finally, the article ends with the conclusion and future work in Section V.

II. SYSTEM BACKGROUND AND ITS WORKING

This paper considers an electric scooter with a wheel-hub BLDC motor for modeling and study purposes. As mentioned in the introduction section, hilly roads consume more energy; hence EVs are less seen in the hilly regions. The motivation behind this paper is to make electric scooters and other EVs more feasible in the hilly regions of the Northeastern part of India. On the hilly roads, some energy spent climbing up can be recovered while climbing down the hill. That is because when the scooter has reached the top of the hill, it has gained potential energy (mgh); while climbing down, some of this energy can be cultivated back into the energy source *i.e.* the battery. The work present in this paper is to show the working of regenerative braking of a wheel-hub motor used in an electric scooter while descending a hill.

A. WORKING OF THE PROPOSED REGENERATIVE BRAKING CIRCUIT CONFIGURATION

The free kinetic motion while descending over the hill slope induces a voltage (back emf) in the motor windings *i.e.*, the BLDC motor now starts behaving like a 3-phase generator. The magnitude of the voltage generated is proportional to the electric vehicle's speed and at a low speed the voltage induced in the motor windings is insufficient to charge the battery directly. For the current to flow from the motor winding to the battery, the voltage must be higher at the input terminal of the battery. Therefore, an intermediary circuit needs to boost the low voltage to a required level, so that, charging of the battery could be achieved during the regenerative braking.

The proposed system will consist of two power-driveline: the first for the motoring mode, *i.e.*, and the normal forward scooter mode; here, the power flows from the battery-inverter-motor as shown in Fig. 4 (b). The second one is for the regeneration mode, which is the regenerative braking action mode, and the power flows from the motor-rectifier-converter-battery, as shown in Fig. 4 (c). The proposed regenerative braking circuit is an add-on circuit to the existing EV motor drive-train. The overall control architecture of the proposed driving system is shown in Fig. 4 (d). The traction system consists of a control hierarchy; the higher level control on a physical level (human level interface) and the lower level control on an electronic level. The regenerative braking process starts when the rider initiates the braking action by pressing the brake button. The brake device can be either a foot-pressed brake pedal or a thumb-pressed pedal mounted on the accelerator throttle; these devices convert the physical brake force into equivalent electrical quantity [28], [36]. The output voltage of the braking device is then scaled into a braking current reference and sent to the ECU block. When the braking command is given, the converter controller gets activated, and the inverter controller is deactivated. The close loop feedback is designed to track the barking current (I^*_{brake}) such that the required braking torque (T_{brake}) is produced and the braking force is available on the wheel-hub motor.

B. MODELING OF BRAKING FORCE, BRAKING TORQUE AND BRAKING CURRENT

While descending the hill, the F_{gh} force, which is the force component due to the weight and the gravitational acceleration, acts as the driving force for the scooter as illustrated in Fig. 4 (a). Here, the F_{gh} assist in the motion of the scooter, and the governing equation for motion without any braking force can be then written as

$$\frac{dv}{dt} = \frac{F_{gh} - (F_f + F_a)}{m} \tag{1}$$

where, v is the scooter speed in m/s, m is the mass of the scooter in kg, F_f is the friction force, F_a aerodynamic drag force and their definitions are given in Appendices III.

From (1), we can see that when the scooter is on a slope with a hill angle (θ), then due to the force $mgsin\theta$, the scooter body will keep accelerating. To prevent the scooter from over speeding a brake force F_{brake} can be applied, the governing equation for motion with brake force is then given as

$$\frac{dv}{dt} = \frac{F_{gh} - (F_f + F_a + F_{brake})}{m} \tag{2}$$

where, F_{brake} is provided by the electric braking circuit.

When the F_{gh} aids the scooter's motion. The wheel-hub BLDC motor experiences a mechanical (load) torque due

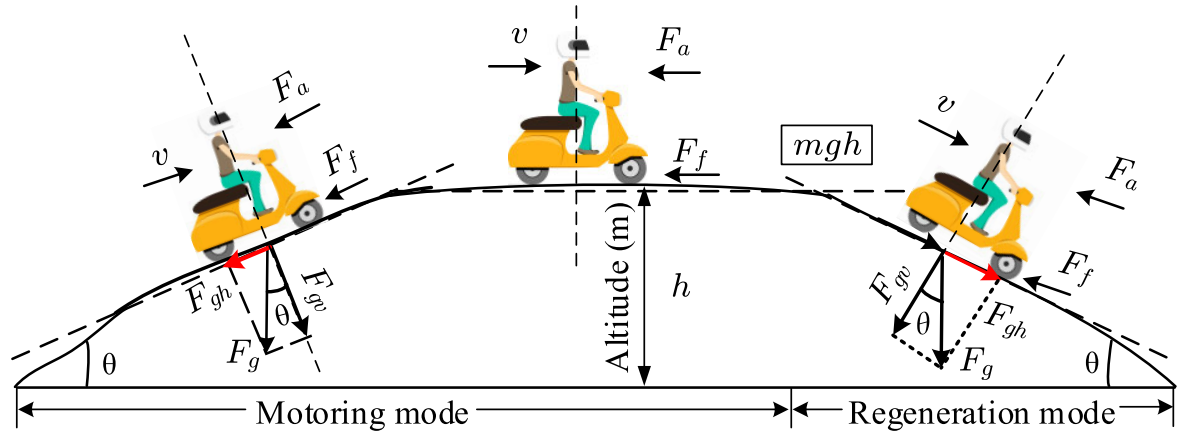

(a)

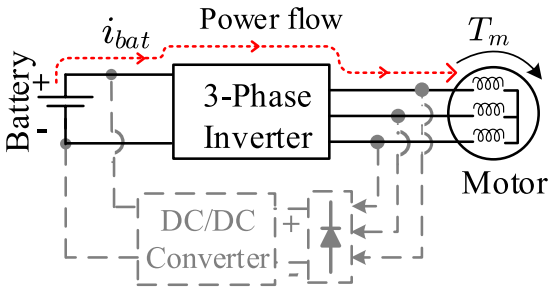

(b)

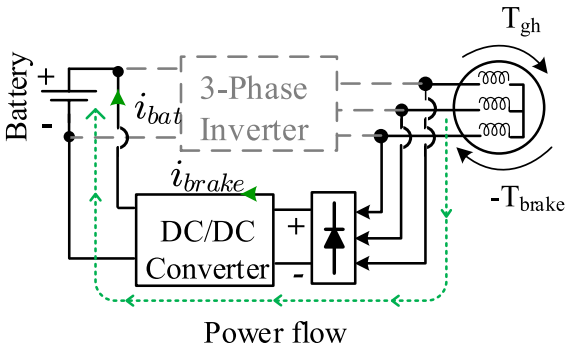

(c)

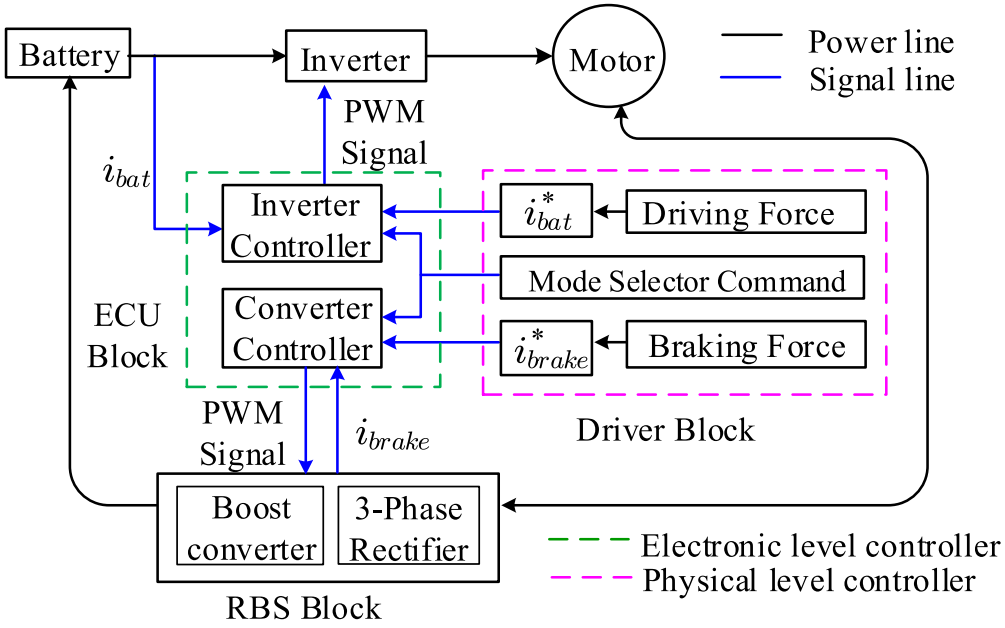

(d)

FIGURE 4. Schematic diagram showing (a) tractive forces associated while climbing up and down a hilly road. (b) circuit configuration of the motoring mode power-drive train (c) circuit configuration of the generator mode power-drive train. (d) Single line diagram of the control architecture showing the control hierarchy.

to F_{gh}. This mechanical torque which aids to the motion of the motor, is then given as

$$T_{gh} = [F_{gh} - (F_f + F_a)]r \tag{3}$$

where, r is the radius of the wheel-hub motor.

The rider provides the braking force (F_{brake}) by pressing an electric brake pedal. The electric brake pedal are a linear hall effect sensor based devices which converts the input force into electrical quantity in volts. The output voltage of the braking device is then scaled into braking current reference (I^*_{brake}).

$$I^*_{brake} = K_b F_{brake} \tag{4}$$

where, K_b is the scaling factor.

The I^*_{brake} and the sensed circuit current from the current sensor is then fed to the close loop feedback circuit of the controller. The braking circuit will draw braking current (I_{brake}) which will developed the electromagnetic torque (T_{brake}) in the motor. T_{brake} is the braking torque developed in the motor which opposes the external driving torque T_{gh} and is given as,

$$T_{brake} = K_t I_{brake} \tag{5}$$

where, K_t is torque constant of the motor.

The negative sign of T_{brake} as shown in Fig. 4 (b) indicates that it is the opposing electromagnetic torque. The magnitude of T_{brake} is proportional to the armature current flowing in the motor winding, I_{brake} is the rms value of the armature current. As shown in Fig. 4 (b), I_{brake} flows from the motor terminal to the rectifier terminal to the converter and then to the source battery.

C. MODELING OF THE PROPOSED REGENERATIVE BRAKING CIRCUIT

The modeling of the main braking circuit *i.e.* the DC/DC boost converter is done considering a DC input voltage V_{in} which is the rectified output voltage of the three phase diode bridge rectifier. The battery is the output (load). Here, in this paper, a simple equivalent electric circuit model of a battery is considered as shown in Fig. 5 (a). The model consist of a source (E_{eq}) and an internal resistance (R_{int}).

In the braking circuit, the energy transfer from the input to the load side is controlled by controlling the turn-on period of the pulse width modulation (PWM) signal provided to the MOSFET switch (S). As shown in Figs. 5 (b) & (c), when S is ON, the braking energy is transferred from the motor line to the inductor by charging it; here, the braking energy is stored in its magnetic field of the inductor (L). When S is OFF, the inductor energy is transferred to the battery that is the inductor is discharged. The energy transfer to the battery over the braking period (neglecting the internal resistance drop losses in the battery) is expressed as

$$E_{bat} = \int_{t_1}^{t_2} (V_{bat} i_{bat}) dt \tag{6}$$

where, V_{bat} is the terminal voltage of the battery and I_{bat} is the battery charging current. The steady-state mean voltage

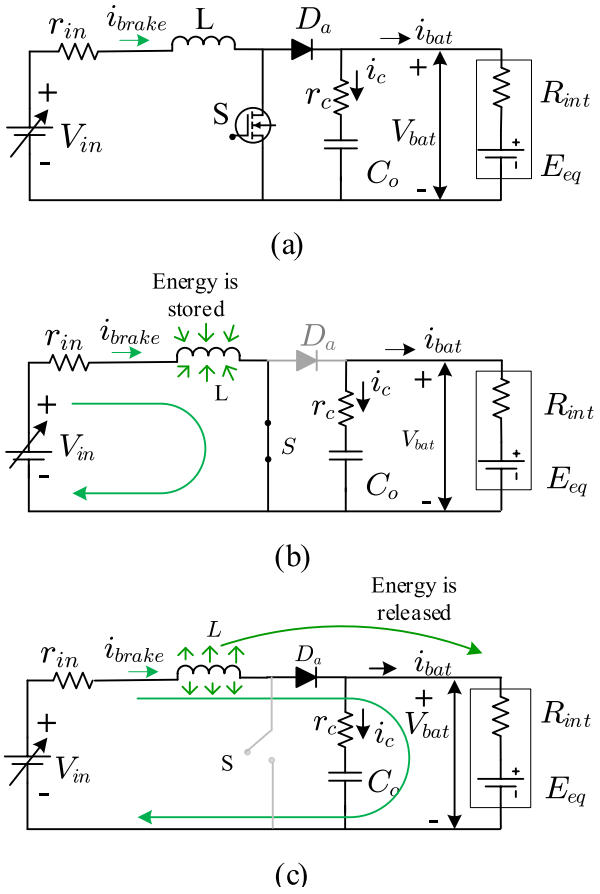

FIGURE 5. Equivalent circuit of (a) DC/DC boost converter (b) when switch is ON, (c) when switch is OFF.

over one switching period is given as

$$V_{bat} = \frac{V_{in} - I_{brake} r_{in}}{(1 - D)}, \quad (0 < D < 1) \tag{7}$$

where, D is the duration of the switch ON period commonly known as the duty ratio.

The mean braking current is derived as

$$I_{brake} = \begin{cases} \dfrac{\frac{V_{in}}{(1-D)^2} - \frac{E_{eq}}{(1-D)}}{R_{int} + \frac{r_{in}}{(1-D)^2}} & (V_{bat} - E_{eq}) \geq 0 \\ 0 & (V_{bat} - E_{eq}) < 0 \end{cases} \tag{8}$$

The battery charging current (I_{bat}) is then expressed as

$$I_{bat} = (1 - D) I_{brake} \tag{9}$$

$$I_{bat} = \begin{cases} \dfrac{\frac{V_{in}}{(1-D)} - E_{eq}}{R_{int} + \frac{r_{in}}{(1-D)^2}} & (V_{bat} - E_{eq}) \geq 0 \\ 0 & (V_{bat} - E_{eq}) < 0 \end{cases} \tag{10}$$

For the dynamic state study a small signal model of the braking circuit with the battery as load was done using state-space averaging technique. The average state-space equations are given as follows.

$$\frac{d\hat{\boldsymbol{x}}}{dt} = A\hat{\boldsymbol{x}} + B\hat{\boldsymbol{u}}_n, \quad \hat{\boldsymbol{y}} = C\hat{\boldsymbol{x}} + D\hat{\boldsymbol{u}}_n \tag{11}$$

where,

$$\hat{\boldsymbol{x}} = \begin{bmatrix} \hat{i}_{brake} & \hat{v}_c \end{bmatrix}^T$$

$$\hat{\boldsymbol{u}}_n = \begin{bmatrix} \hat{v}_{in} & \hat{E}_{eq} & \hat{d} \end{bmatrix}^T, \quad \hat{\boldsymbol{y}} = \begin{bmatrix} \hat{i}_{brake} & \hat{v}_{bat} \end{bmatrix}^T$$

$$A = \begin{bmatrix} -\frac{1}{L}(r_{in} + R_1 D') & -R_2 \frac{D'}{L} \\ R_2 \frac{D'}{C_{out}} & -\frac{1}{C(r_c + R_{int})} \end{bmatrix}$$

$$B = \begin{bmatrix} \frac{1}{L} & -R_3 \frac{D'}{L} & R_1 \frac{I_{brake}}{L} + R_2 \frac{V_{bat}}{L} + R_3 \frac{E_{eq}}{C} \\ 0 & \frac{1}{C(r_c + R_{int})} & -R_3 \frac{I_{brake}}{C} \end{bmatrix}$$

$$C = \begin{bmatrix} 1 & 0 \\ R_1 D' & R_2 \end{bmatrix}, \quad D = \begin{bmatrix} 0 & 0 & 0 \\ 0 & R_3 & -R_1 I_{brake} \end{bmatrix}$$

where,

$$R_1 = \frac{r_c R_{int}}{(r_c + R_{int})}, \; R_2 = \frac{R_{int}}{(r_c + R_{int})}, \; R_3 = \frac{r_c}{(r_c + R_{int})}$$

The transfer function (TF) of the converter can be obtained by taking Laplace TF of the of (11) and is given by

$$\hat{Y}(s) = (C(sI - A)^{-1}B + D)\hat{u}_n(s)$$

Using the converter parameters given in Appendices I, the duty cycle to braking current TF is given as

$$G_p(s) = \frac{\hat{i}_{brake}(s)}{\hat{d}(s)} = \frac{8.929 \times 10^4 s + 1.082 \times 10^8}{s^2 + 1122\, s + 1.524 \times 10^5} \quad (12)$$

With the plant TF (12) derived, next a feedback system is designed to vary the converter's control input (i.e., the duty cycle) such that the braking current of the circuit is regulated to follow the reference braking current for varying input voltage.

D. CONTROLLER DESIGN

The dynamic state control design includes

- The switching between motoring and regeneration mode
- Controller design to track the braking current reference

1) SWITCHING BETWEEN TWO MODES

The motor drive controller and the regenerative braking circuit controller are designed to be complementary, meaning only one mode will be active at any given moment; the algorithm is outlined in Fig. 6 (a). This control is done on the physical level, i.e. with human involvement. The rider initiates the braking action by pressing the brake pedal or pressing a switch button mounted on the accelerator throttle. Once the rider gives the signal, the regenerative braking mode action begins. The logic gate is shown in Fig. 6 (b) which enable or disable the gate pulse to the switch.

2) CURRENT CONTROL OF THE BRAKING CIRCUIT

The close loop current control of the braking circuit is presented in this section. Fig. 7 (a) shows the block diagram of the closed-loop system, where G_C denotes controller transfer function (TF), G_M denotes PWM TF and

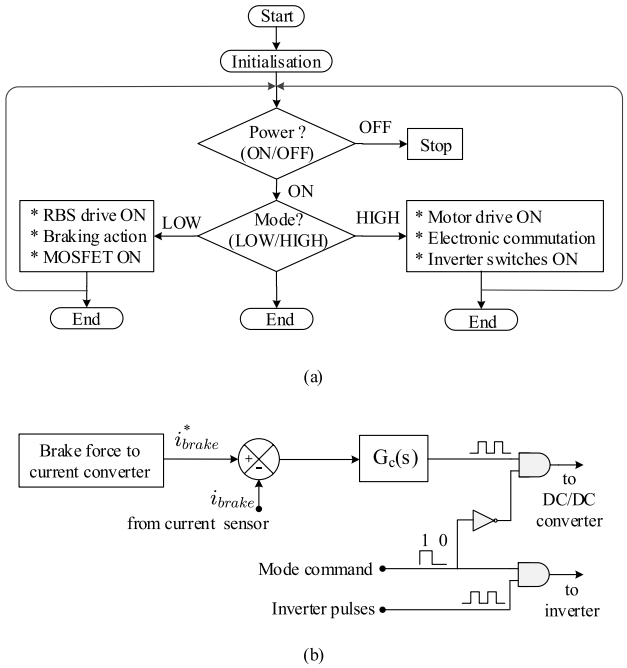

FIGURE 6. Algorithm design to switch between the two modes (a) flow chart (b) its implementation with logic gates.

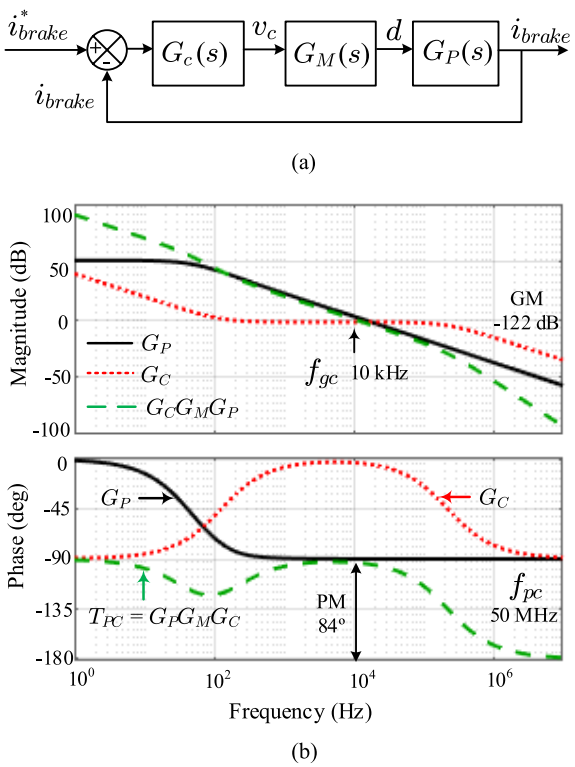

FIGURE 7. Converter current-control (a) close-loop control system (b) bode plot of G_P, G_C and $G_P G_C G_M$.

G_P denotes current-control plant TF. The G_P is derived using the small-signal modeling as given in (12).

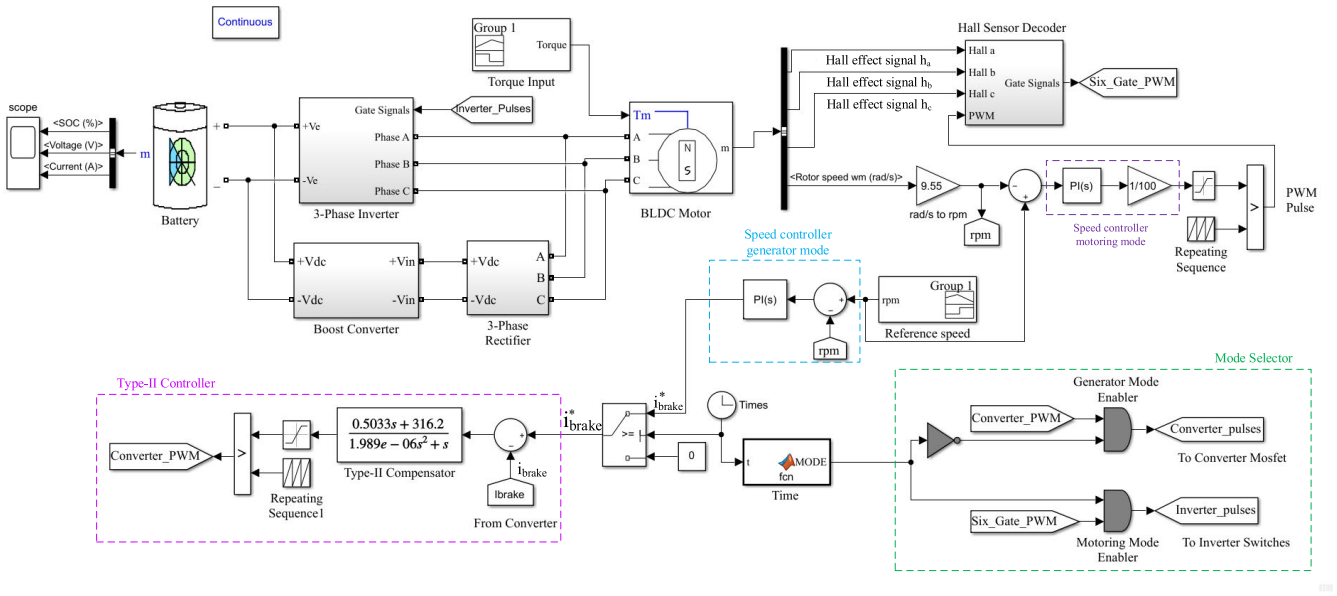

FIGURE 8. MATLAB/Simulink simulation screenshot of the regenerative braking system configuration along with its controller.

To regulate I_{brake} to I^*_{brake}, the overall gain of the loop gain TF ($G_C G_M G_P = T_{PC}$) should be high. Here, Type-II compensator is chosen as the controller. The TF of G_C and G_M is given by

$$G_C(s) = \frac{k_c(1+\frac{s}{\omega_z})}{s(1+\frac{s}{\omega_p})} \quad \& \quad G_M = \frac{1}{V_M} \tag{13}$$

where, k_c, ω_z, ω_p are the controller gain, controller zero and controller pole respectively and V_M is the peak voltage of ramp signal. The design criteria in placing the controller pole and zero is such that the loop gain TF crossover frequency should be high with phase margin (PM) greater than 45° and gain margin (GM) greater than 20 dB. These criteria ensure good stability and transient performances. Therefore, the crossover frequency is chosen at 10 kHz, which is 1/10th of switching frequency (f_s = 100 kHz). To achieve PM = 84° at gain crossover frequency, f_{gc} = 10 kHz, the controller parameter are calculated using

$$|G_C G_M G_P|_{f_{gc}} = 1 \quad \& \quad \angle G_C G_M G_P = -180 + \text{PM} \tag{14}$$

The designed Type-II compensator for the converter at f_{gc} = 10 kHz and taking the converter parameter given in Appendix I is then computed as

$$G_c(s) = \frac{0.5033s + 316.2}{1.989 \times 10^{-06}s^2 + s} \tag{15}$$

Fig. 7 (b) shows the bode plot of compensated TF (T_{PC}), controller TF (G_C) and uncompensated plant TF (G_P). From the bode plots it is observed that with the designed compensator the desired PM = 84° at f_{gc} = 10 kHz is achieved and the low frequency gain is high. This will ensure us a good steady state, transient response and good stability.

III. SIMULATION STUDY

This section verifies the control strategy and Type-II current compensator designed in the preceding section via simulation in the MATLAB/Simulink environment. The simulation aims to show the dynamic response of the proposed regenerative braking circuit and validate its working as a topology. Fig. 8 shows the arrangement of the inverter model, BLDC motor, rectifier, and Li-Ion battery blocks taken from the MATLAB/Simulink library. The various parameters for the BLDC motor and boost converter used for the simulation are given in the Appendices II. Since simulating the complete vehicle drive-line is out of the scope of this paper, here are some initial settings and assumptions made for the simulation study:

- The BLDC motor is driven with mechanical torque (T_m) as its input. The T_m is positive during the motoring mode, and for the regenerative mode, T_m is negative. This negative T_m emulates the effect of T_{gh} due to the F_{gh}. T_{gh} force is assumed to be a constant force during the regenerative mode. Using MATLAB/Simulink signal builder block, the load torque is predefined.
- In the real-world physical drive scenario, the rider is both the reference speed generator and the regulator. Depending on the brake force given by the rider, the speed is slowed and maintained. For the simulation purpose, to emulate the rider's braking action, a PI controller block is used to regulate the speed to produce the braking current reference from the difference between the actual motor speed and the reference speed input. The desired reference motor speed is generated using a signal builder.

- The simulation is for a short 6 s, just enough to show the dynamic behaviours. That is because of power electronics components like the MOSFET with a switching frequency of 100 kHz; the simulation time step is 1×10^{-6}, which slows the computational speed.

Fig. 9 shows the various waveforms of the simulated dynamic responses. Fig. 9 (a) plots the mode command signal input, which is the command given to the controller to switch between motoring mode and the regeneration mode. As seen from Fig. 9 (a), initially, the mode signal is HIGH, indicating the motoring mode, *i.e.*, the normal forward motion. Here, in this mode, the motor controller is active, and the inverter pulses are ON while the regenerative braking circuit is inactive and the converter pulses are OFF. Then, at 2 s, the mode signal is turned LOW, indicating regeneration mode is ON. Here, in this mode, the regenerative braking circuit is active, and the converter pulses are ON while the inverter pulses are OFF, and the motor controller is inactive. Then again, at 4.5 s, the system is back to motoring mode. This shows that the control strategy given to the simulation system to swap between motoring and regeneration mode is working and effective.

Other than the mode command signal, the simulation has two predefined inputs: T_m and ω_m^* as shown with dotted lines in Figs. 9 (b) and (c), respectively. As seen from the Fig. 9 (b) plot during the motoring mode, the T_m is a positive 3 Nm which acts as the load to the motor. At 2 s, when the regeneration braking commences, the T_m is -3 Nm; the negative T_m value emulates the effect of the free torque due to the gravitational acceleration force F_{gh}. The motor generates T_{brake} equal to $k_t I_{brake}$ to reach the desired speed. The response waveform of T_{brake} is shown in Fig. 9 (b).

At 2 s, the regenerative braking commences upon receiving the braking command and braking force applied by the rider. The converter controller then tracks the braking current reference. The desired braking current starts flowing in the circuit, generating the desired braking torque required to oppose T_{gh} due to the slope. As seen from Figs. 9 (b) and (d) for $T_{gh} = -3$ Nm input, the braking current drawn is 2.6 A (T_{gh}/k_t; $k_t = 1.165$) and braking torque 3 Nm is generated.

Due to the opposing electromagnetic braking torque, the speed of the motor drops from 242 rpm to 225 rpm as shown in Fig. 9 (c). The voltage generated corresponding to 225 rpm is 25 V, as shown in Fig. 9 (e). The duty cycle generated by the converter controller is 0.46. The boost converter will boost the input voltage 25 V to a voltage slightly higher than the battery voltage (42 V, SOC 30%) so that the required current can flow to charge the battery.

Fig. 9 (d) plots the braking current and the battery charging current respectively. The negative battery current indicates the charging of the battery, which can also be validated from the battery SOC profile given in Fig. 9 (f). During the motoring period the SOC decreases as the power is supplied for the traction effort and during the regenerative braking mode the

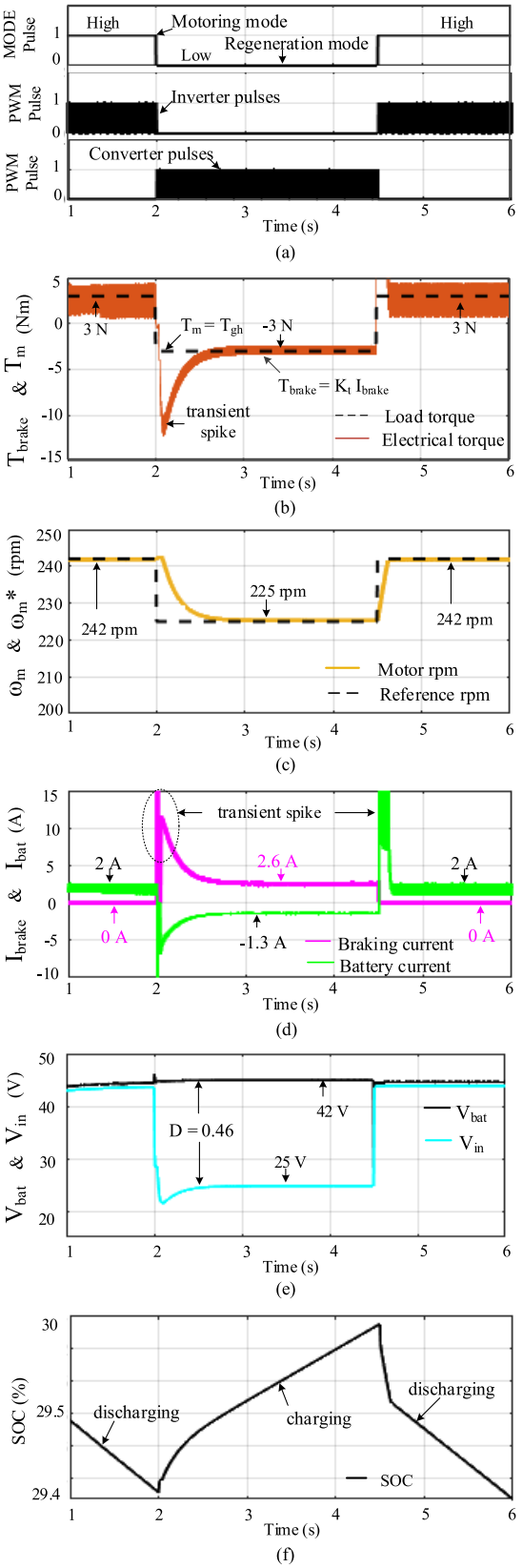

FIGURE 9. Simulated dynamic response waveforms. (a) mode selector signal, inverter pulses, and converter pulses. (b) T_m and T_{brake}. (c) ω_m and ω_m^*. (d) I_{brake} and I_{bat}. (e) V_{in} and V_{out}. (f) battery SOC.

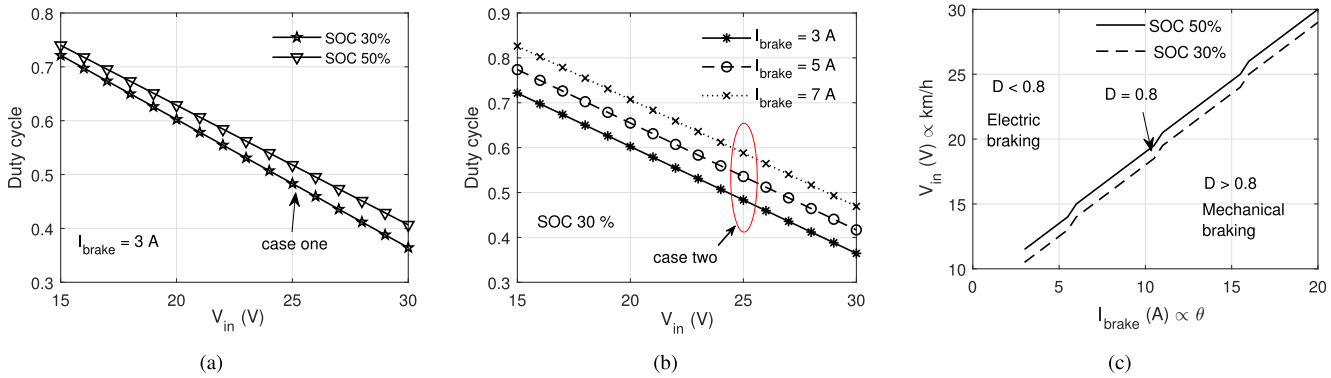

FIGURE 10. Steady-state calculated results showing; (a) duty cycle D as function of input voltage V_{in} at fixed value of braking current I_{brake}, (b) and at different value I_{brake}. (c) shows the minimum speed the scooter should attained for a given hill angle for the regenerative circuit to function.

SOC is increasing indicating there is rise in the charge in the battery.

The above discussion shows that the control strategy (mode selection) and Type-II compensator performs as desired by the designer. The dynamic response shows that the designed controller gives us a good transient response, steady-state performance, and stability. The simulation results validates that the proposed regenerative braking circuit topology effectively tracks the braking current and generates the braking torque to slow down the speed of the motor and simultaneously charge the battery.

A. STEADY-STATE ANALYSIS AND DISCUSSION

In the steady-state condition, whistle braking action, the scooter descends the slope at a comfortable speed due to the applied brake torque and simultaneously charges the battery. The steady-state modulation of the duty cycle is presented in this section. From (7), the duty cycle (D) is then derived as

$$D = \frac{V_{bat} - V_{in} + (I_{brake} r_{in})}{V_{bat}} \tag{16}$$

From (9), we see that the charging current is a function of the duty cycle of the PWM signal and the braking current. Again from (16), it is seen that the value of the duty cycle is a function of the input voltage of the converter (proportional to the speed of the scooter), the braking current drawn, the available battery voltage, which in turn is dependent on the state of charge (SOC) of the battery. The value of the duty cycle is then a multivariable dependent.

The duty cycle of the regenerative braking circuit as a function of the input voltage, battery voltage and braking current is presented here by taking two different cases. Case one is the scenario of the scooter descending at a different speed (30 km/h, 25 km/h, 20 km/h, and 15 km/h) while drawing a braking current (3 A). For case two, the scooter speed is fixed (25 km/h) while drawing different braking currents (3 A, 5 A, and 7 A). The braking circuit sees different input voltages due to varying speeds in case one, while it will see the same input voltage value in case two for the same speed. Here, for simplicity, the magnitude of V_{in} is considered directly proportional to the scooter speed, and the braking current is proportional to the braking torque requirement. The duty cycle calculation for both cases using the equation (16) is given in Table 2 and 3.

Table 2 shows the results of case one. For the same I_{brake}, with the decrease in V_{in} value, the duty cycle increases, and the efficiency of the boost converter decreases. The I_{bat} reduces with an increase in the duty cycle for the same I_{brake}. Table 2 tells us that the power transfer and energy recovery are more efficient with higher descending speed for the same braking current. Fig. 10 (a) plots case one; it plots the calculated duty cycle vs. V_{in} for a fixed I_{brake} for two different battery voltages.

TABLE 2. Case one: Different scooter speed with same braking current.

V_{in} (V)	P_{in} (W)	SOC 50% (V_{out} = 45 V)				SOC 30% (V_{out} = 42 V)			
		D	I_{bat} (A)	P_{out} (W)	η (%)	D	I_{bat} (A)	P_{out} (W)	η (%)
30	90	0.40	1.80	81	90	0.36	1.92	86.4	96
25	75	0.51	1.47	66	88	0.48	1.56	70.22	93
20	60	0.62	1.14	51	85	0.60	1.20	54.0	90
15	45	0.74	0.78	35	77	0.72	0.82	37.0	82

TABLE 3. Case two: Same scooter speed with different braking current.

I_{brake} (A)	P_{in} (W)	SOC 50% (V_{out} = 45 V)				SOC 30% (V_{out} = 42 V)			
		D	I_{bat} (A)	P_{out} (W)	η (%)	D	I_{bat} (A)	P_{out} (W)	η (%)
3	75	0.52	1.44	64.80	86	0.48	1.56	66	88
5	125	0.57	2.15	96.75	77	0.53	2.35	96.6	79
7	175	0.62	2.66	120.0	68	0.58	2.95	122	75

Similarly, from Table 3 which shows the calculation for case two, it is seen that for the same scooter speed 25 km/h and $V_{in} = 25$ V, with the increase in I_{brake} demand from 3 A to 7 A, the duty cycle value also increases, and the efficiency reduces. Fig. 10 (b) plots case two; it plots the duty cycle vs. V_{in} for a fixed battery voltage and three different I_{brake}. Since T_{brake} is required to oppose the T_{gh}, then the I_{brake} requirement also increases with the hill angle. Here, it is

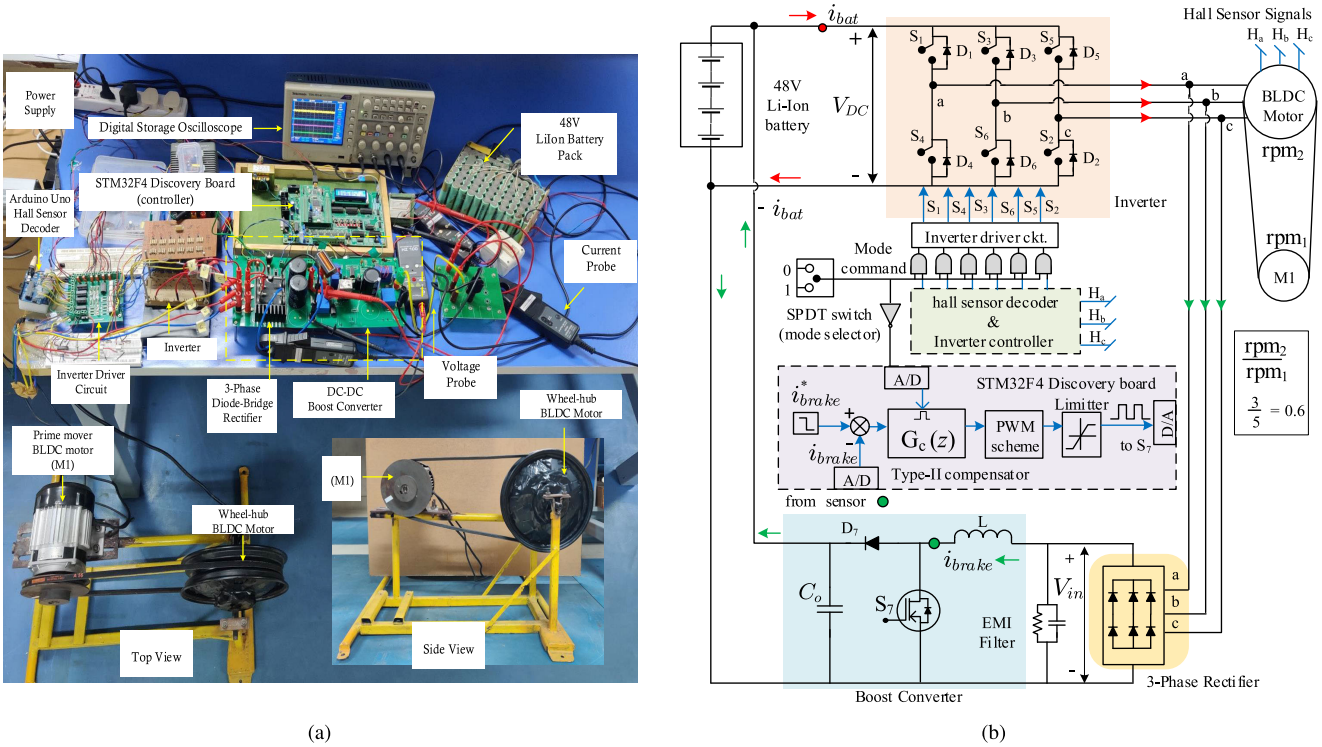

FIGURE 11. Hardware set-up (a) laboratory experimental test set-up. (b) detailed schematic equivalent circuit connection of the experimental test set-up.

inferred that even though there is more potential energy to harvest on the road with a higher hill angle and steeper slopes, it always does not result in more energy recovery, the reason being that the rider generally tends to slow down on the steeper slope, resulting in the low input voltage. Steeper the slope higher the brake force and braking current requirement.

From the steady-state analysis of cases one and two, it is inferred that the speed of the scooter (proportional to the input voltage) and the slope of the road (proportional to the braking current) affect the duty cycle of the converter in a contradicting manner. Since input voltage is inversely proportional to the duty cycle and the braking current is directly proportional to the duty cycle, then for a given hill angle, there is a minimum speed limit below which the duty cycle crosses 0.8. This speed value at which the duty cycle hits 0.8 is a critical point beyond which it is wiser to switch to mechanical braking. For higher efficiency, a DC/DC boost converter's duty cycle is usually operated below 0.8 [42]. Fig. 10 (c) plots input voltage/speed vs. the braking current/slope at the value where D hits 0.8. Here, V_{in} is calculated as a function of I_{brake} at D equal to 0.8 by using (16). The V_{in} value tells the minimum speed for the scooter on a hilly road for a given hill angle value for the boost converter to work efficiently.

IV. EXPERIMENTAL RESULTS

The proposed regenerative braking circuit to harvest potential energy has been typed tested on an experimental table set up in the laboratory. Fig. 11 (a) shows the hardware setup, and Fig. 11 (b) shows its schematic layout of the hardware connection. The experimental design is for a reduced power scale. The motoring mode powertrain consists of a Li-Ion battery pack (48 V, 12 Ah), a 3-phase in-wheel BLDC hub motor (1.8 kW), a 3-phase inverter module and an inverter driver circuit. For the motoring mode controller, Arduino Uno is implemented, which generates the PWM signal and also decodes the three hall sensors to provide the six commutation state for the inverter during the motoring mode.

The regenerative braking circuit consists of a 3-phase rectifier, DC/DC boost converter, signal conditioning circuit, and an STM32F4 Discovery kit as the controller, which generates the PWM for the MOSFET of the converter circuit. The swapping between motoring and regeneration mode is actualized by an SPDT switch as shown in Fig. 11 (b); by default, it is in the HIGH state (motoring mode), then via a NOT gate, the converter controller is on a LOW state. When the switch is made LOW, the motoring mode gets deactivated, and the converter controller gets a HIGH signal via the NOT gate, which starts the regenerative braking action. Here, Matlab/Simulink Waijung blockset was used to generate the code for the controller. Waijung is an embedded coder target that enables code generation for the STM32F4 Discovery kit, i.e. it easily deploys the MATLAB/Simulink models to the hardware controller. A continuous to discrete conversion by standard bilinear transformation method was performed on MATLAB to convert the Type-II controller TF in (15) with a sampling time of 5 kHz. The discretized Type-II

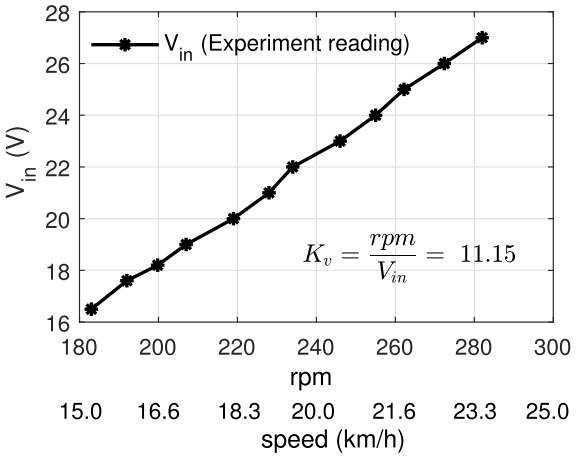

FIGURE 12. Voltage relationship with motor rpm and scooter speed.

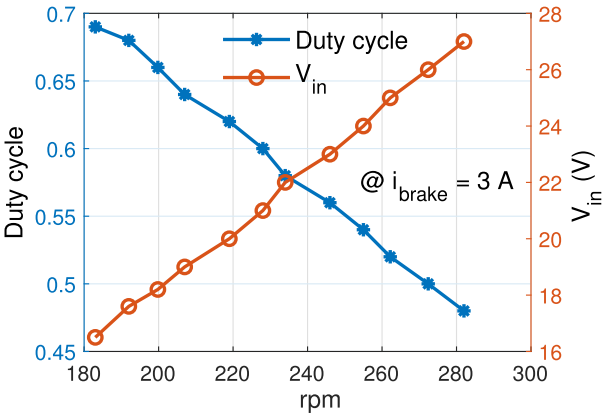

FIGURE 13. Duty cycle variation for fixed braking current and varying motor rpm.

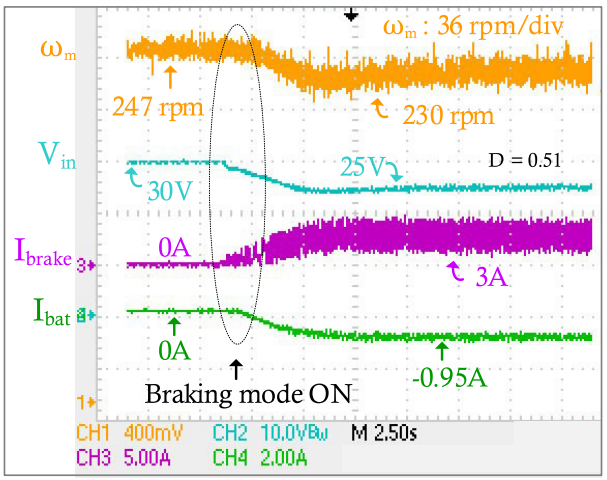

FIGURE 14. Experimental results showing the braking action from 247 rpm to 230 rpm with 3A braking current.

controller TF is then derived as

$$G_c(z) = \frac{0.5245z^2 + 0.06201z - 0.4625}{z^2 - 0.03901z - 0.961} \tag{17}$$

Next, to emulate the downhill driving condition, another BLDC motor, powered by another set of a 48 V battery and a 3-phase inverter, is used. This BLDC motor acts as the prime mover machine to provide free rotating motion due to the hill angle. The prime mover BLDC motor is denoted as M1, and its speed is controlled with a potentiometer; it is connected to the BLDC hub motor through a belt, as shown in Fig. 11 (b). The ratio between the wheel hub motor to the M1 is 0.6.

A. EXPERIMENT TO FIND THE MOTOR RPM VS. V_{in}

The characteristic of wheel hub BLDC motor speed and its induced voltage (rms) is studied by conducting a simple experiment in a no-load condition. From a potentiometer, the speed of the M1 is varied. M1 motor drives the BLDC hub motor through the belt at different speeds, and the corresponding induced voltage across the three-phase rectifier was measured using a voltmeter. Fig. 12 shows the measured values of the induced voltage (rms), which is the V_{in} to the boost converter. On the y-axis of Fig. 12 is the V_{in} corresponding to the wheel-hub motor rpm, and on the x-axis of the graph is the motor rpm. The estimated scooter speed, which was calculated using the relationship (18) is also shown below the motor rpm.

$$\text{Scooter speed in km/h} = (\text{rpm})\left(\frac{\pi}{30}\right) \text{r} \left(\frac{3600}{1000}\right) \tag{18}$$

The voltage induced is proportional to the scooter's speed. The voltage constant (K_v) for this motor is 11.15.

B. EFFECT OF MOTOR RPM ON DUTY CYCLE

Next, the boost converter and the Li-Ion battery are connected to the rectifier output. The braking current reference was fixed at 3 A, which means the braking torque generated is also fixed. The speed of the wheel-hub motor is varied from 180 rpm to 282 rpm, generating varying V_{in} from 16 V to 27 V. The controller of the boost converter regulates the PWM duty cycle accordingly to boost V_{in} to get the required $I_{brake} = 3$ A *i.e.*, same braking torque. When the speed is 282 rpm, 0.48 of the PWM duty can boost V_{in} to get the required $I_{brake} = 3$ A and when the when the speed is 180 rpm then 0.69 will do the same as plotted in Fig. 13. These results correspond with the theoretical analyses of the steady-state study.

C. DSO CAPTURE OF THE DYNAMIC BEHAVIOUR

Here in the DSO captured experimental results, the Yellow waveform corresponds to the wheel-hub motor speed response. The Cyan waveform is for the input voltage response, the Magenta waveform is for the current braking response, and the Green waveform is for the battery current.

In Fig. 14, initially, the wheel hub motor is freely rotated at 247 rpm, and both the motoring mode circuit and the generator mode circuit are inactive. Then after some moment has elapsed, the regenerative braking circuit is turned ON by manually switching the SPDT switch. The DC/DC current controller regulates itself to track the reference current, set

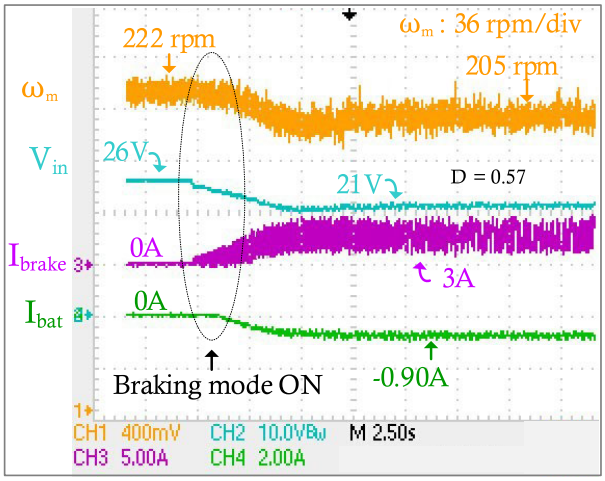

FIGURE 15. Experimental result showing the motoring and braking mode from 222 rpm to 205 rpm with 3A braking current.

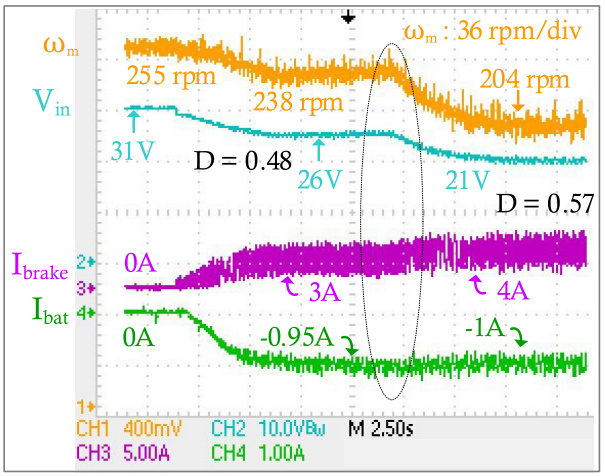

FIGURE 17. Experimental results showing the braking action from 238 rpm to 204 rpm with a step-change in the barking current reference from 3A to 4A.

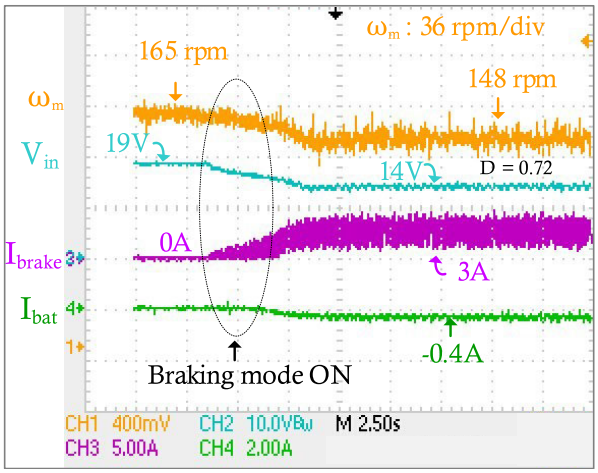

FIGURE 16. Experimental results showing the braking action from 165 rpm to 148 rpm with 3A braking current.

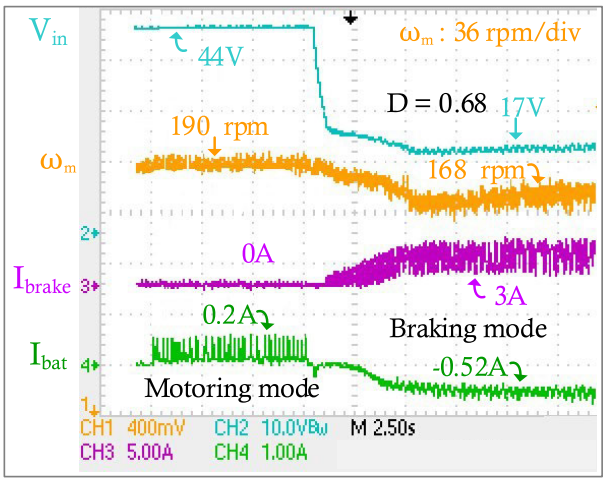

FIGURE 18. Experimental result showing transition between the motoring mode and braking mode.

at 3 A. It can be observed from the speed waveform that as the braking circuit draws a 3 A current, the speed drops to 230 rpm from 247 rpm. The 3 A current generates a reverse torque, which opposes the free mechanical torque, decreasing the motor speed. The boost converter sees an input voltage of 25 V for 230 rpm. The duty cycle of the PWM was measured to be 0.51 for input voltage 25 V and battery voltage 44 V. Similarly, keeping everything else same Fig. 15 and Fig. 16 are the captures for different motor speeds. It is inferred from the Fig. 14, Fig. 15 and Fig. 16 that for the same braking current, the higher motor speed results in higher recovery of energy. A higher charging current flow is possible with higher input voltage, since the battery charging current increases with the decrease in the duty cycle for the same braking current.

Fig. 17 shows the capture of a case of a step-change in the braking current reference. It is seen from the motor speed plot that as the braking current increases from 3 A to 4 A, the motor speed decreases from 238 rpm to 204 rpm. The controller regulates the duty cycle from 0.48 to 0.57 as the voltage input drops from 26 V to 21 V to boost it to battery voltage level. This figure validates the Type-II compensator controller's performance to track the change in reference current.

Fig. 18 shows the successful transition between the motoring and regenerative braking modes. Initially, the set-up is run at the motoring mode at no-load condition, a 0.20 duty ratio is given to the inverter pulses. It is seen during the motoring mode the motor-driveline draws a no-load positive battery current of 0.2 A, which is pulsating in nature. During the motoring mode, zero braking current flows as the regenerative braking circuit is at OFF state. Once the regenerative mode command is given, the braking current starts flowing, and the battery current becomes negative, indicating the charging of the battery. The braking current generates the braking torque, due to which the speed drops

from 190 rpm to 168 rpm. Hence, we can see that switching between the two modes is fast and effective.

In conclusion, the experimental results validate the fast switching technique between the two driving modes, i.e., motoring and regenerating. The hardware implementation of the Type-II compensator performs satisfactorily by tracking the reference current and providing the required braking torque. The transient response (in the DSO results captures) shows that the compensator gives us a good transient response, steady-state performance, and stability. Overall the results from Fig. 14 to Fig. 18 validate the feasibility and operation of the proposed regenerative braking system, and its control.

V. CONCLUSION

This paper has proposed a regenerative braking circuit that is modular and can be integrated into existing electric scooter which uses mechanical braking. It offers fast switching between the two driving modes, i.e., motoring and regenerative braking, by enabling or disabling the gate pulses to the inverter or the boost converter. This switching method increases reliability and reduces the cost of the circuit by eliminating power switches to switch between motoring and regenerative braking modes. Since the proposed regenerative system uses the same source battery for both driving modes, i.e., motoring and regenerative braking, thus reducing the cost and weight of additional energy sources.

In motoring mode, the switches used in the inverter circuits are typically in the range of 10 kHz; hence, the Type I regenerative braking circuit uses approximately the same frequency for regenerative braking. Thus increasing the ripple in current and reducing the voltage gain. Whereas the proposed configuration uses a separate braking circuit, the braking circuit is designed at 100 kHz, thus increasing the voltage gain and is suitable for low-speed braking. The feasibility and the working of the proposed regenerative braking circuit are validated through simulations in MATLAB/Simulink. Further, the results are also experimentally verified on a developed prototype of a scaled-down laboratory test set-up. The results show successful braking action and the charging of the battery at a very low speed in the range of 25 km/h to 15 km/h, as required on hilly roads. These results also validate the compensator design used in the boost converter, which is the power-transferring circuit of the regenerative braking system. Overall this paper contributes to the design, analysis, modelling, simulation and novel hardware technique implementation of the control scheme and working of the proposed modular regenerative braking system. Further, the present work can be extended by including the energy efficiency study of the regenerative braking system.

APPENDICES

I BOOST CONVERTER PARAMETERS

Switching frequency (f_s) = 100 kHz; Inductor (L) = 0.56 mH; Capacitor (C_{out}) = 2700 μF; r_{in} = 0.05 Ω, r_c = 0.01 Ω, R_{int} = 0.33 Ω.

II BLDC MOTOR PARAMETERS

Stator resistance (R_s) = 0.11Ω; Stator inductances (L_s) = 0.25 mH; Voltage constant (K_v) = 122 $V_{l-l}/krmp$; Torque constant (K_t) = 1.165 (Nm/A); Inertia (J) = 0.35; No. of pole pair = 24.

III VEHICLE DYNAMICS

The resistive force the electric scooter has to overcome to be in motion is called the tractive effort. These tractive resistive forces are shown in Fig. 4 (a). During normal forward motion (motoring mode), the source battery should supply power to overcome these tractive resistive forces. The total tractive resistive force (F_t) is then given as

$$F_t = F_f + F_a + F_{gh} + m\frac{dv}{dt} \tag{19}$$

where, F_f is the friction force to overcome the rolling resistance between tire and road surface and is given as

$$F_f = \mu_{rr} mgcos\theta \tag{20}$$

where, m is the mass of scooter in kg, and the passenger, μ_{rr} is the rolling friction coefficient. The value of μ_{rr} varies with different types of the road; here, the value taken is for an asphalt concrete surface road.

The aerodynamic drag force is expressed as

$$F_a = \frac{1}{2}\rho A C_d v^2 \tag{21}$$

where, ρ is air density and C_d the drag coefficient whose value depends on the vehicle's design. Two-wheelers such as motorcycle and scooters have much higher values of C_d than four-wheelers [43].

The effort to climb the hill is denoted as F_g, then, F_{gh} is the vertical force component of F_g due to its weight and gravitational acceleration, which is in horizontal to the road plane as shown in Fig. 4 (a) is given as

$$F_{gh} = mgsin\theta \tag{22}$$

where, g is the universal gravitational acceleration constant and θ the gradient of the road or hill angle. It is to mention here that this force is absent for a plain road drive as hill angle will be zero or close to zero. F_{gh} is negative when descending the hill and aids in the motion of the scooter.

The linear acceleration force is given by $m\frac{dv}{dt}$ where, $\frac{dv}{dt}$ is the acceleration, it is negative during de-acceleration. This force is absent when the vehicle runs at a constant speed.

REFERENCES

[1] A. Emadi, "Transportation 2.0," *IEEE Power Energy Mag.*, vol. 9, no. 4, pp. 18–29, Jul. 2011.
[2] L. Paoli and T. Gül. (2022). Electric Cars Fend Off Supply Challenges to More Than Double Global Sales. IEA. Paris, France. [Online]. Available: https://www.iea.org/commentaries/electric-cars-fend-off-supply-challenges-to-more-than-double-global-sales
[3] A. Emadi, *Advanced Electric Drive Vehicles*. Boca Raton, FL, USA: CRC Press, 2015.
[4] T. Nama, A. K. Gogoi, and P. Tripathy, "Low power electric two-wheelers for hilly region," in *Proc. IEEE Int. Conf. Power Electron., Drives Energy Syst. (PEDES)*, Dec. 2018, pp. 1–6.

[5] S. C. Yang, M. Li, Y. Lin, and T. Q. Tang, "Electric vehicle's electricity consumption on a road with different slope," *Phys. A, Stat. Mech. Appl.*, vol. 402, pp. 41–48, May 2014.
[6] T. Nama, P. Tripathy, and A. K. Gogoi, "Study of hilly region road for electric scooters," in *Proc. IEEE Transp. Electrific. Conf. (ITEC-India)*, Dec. 2021, pp. 1–6.
[7] P. Kadav and Z. D. Asher, "Improving the range of electric vehicles," in *Proc. Electr. Vehicles Int. Conf. (EV)*, Oct. 2019, pp. 1–5.
[8] I. Aharon and A. Kuperman, "Topological overview of powertrains for battery-powered vehicles with range extenders," *IEEE Trans. Power Electron.*, vol. 26, no. 3, pp. 868–876, Mar. 2011.
[9] Z. Li, A. Khajepour, and J. Song, "A comprehensive review of the key technologies for pure electric vehicles," *Energy*, vol. 182, pp. 824–839, Sep. 2019.
[10] S. M. A. S. Bukhari, J. Maqsood, M. Q. Baig, S. Ashraf, and T. A. Khan, "Comparison of characteristics—Lead acid, nickel based, lead crystal and lithium based batteries," in *Proc. 17th UKSim-AMSS Int. Conf. Modeling Simulation (UKSim)*, Mar. 2015, pp. 444–450.
[11] E. Chemali, M. Preindl, P. Malysz, and A. Emadi, "Electrochemical and electrostatic energy storage and management systems for electric drive vehicles: State-of-the-art review and future trends," *IEEE J. Emerg. Sel. Topics Power Electron.*, vol. 4, no. 3, pp. 1117–1134, Sep. 2016.
[12] J.-Y. Kim, B.-S. Lee, Y.-J. Lee, and J.-K. Kim, "Integrated multi mode converter with single inductor for fuel cell electric vehicles," *IEEE Trans. Ind. Electron.*, vol. 69, no. 11, pp. 11001–11011, Nov. 2022.
[13] C. Riczu and J. Bauman, "Implementation and system-level modeling of a hardware efficient cell balancing circuit for electric vehicle range extension," *IEEE Trans. Ind. Appl.*, vol. 57, no. 3, pp. 2883–2895, May 2021.
[14] Y. Xie, C. Wang, X. Hu, X. Lin, Y. Zhang, and W. Li, "An MPC-based control strategy for electric vehicle battery cooling considering energy saving and battery lifespan," *IEEE Trans. Veh. Technol.*, vol. 69, no. 12, pp. 14657–14673, Dec. 2020.
[15] S. Madichetty, S. Mishra, and M. Basu, "New trends in electric motors and selection for electric vehicle propulsion systems," *IET Electr. Syst. Transp.*, vol. 11, no. 3, pp. 186–199, Sep. 2021.
[16] J. de Santiago, H. Bernhoff, B. Ekergård, S. Eriksson, S. Ferhatovic, R. Waters, and M. Leijon, "Electrical motor drivelines in commercial all-electric vehicles: A review," *IEEE Trans. Veh. Technol.*, vol. 61, no. 2, pp. 475–484, Feb. 2012.
[17] Y. Zhang, Y. Zhang, Z. Ai, Y. L. Murphey, and J. Zhang, "Energy optimal control of motor drive system for extending ranges of electric vehicles," *IEEE Trans. Ind. Electron.*, vol. 68, no. 2, pp. 1728–1738, Feb. 2021.
[18] N. Huda, S. Kaleg, A. Hapid, M. R. Kurnia, and A. C. Budiman, "The influence of the regenerative braking on the overall energy consumption of a converted electric vehicle," *Social Netw. Appl. Sci.*, vol. 2, no. 4, pp. 1–8, Apr. 2020.
[19] B. Long, S. Lim, J. Ryu, and K. Chong, "Energy-regenerative braking control of electric vehicles using three-phase brushless direct-current motors," *Energies*, vol. 7, no. 1, pp. 99–114, Dec. 2013.
[20] G. Xu, W. Li, K. Xu, and Z. Song, "An intelligent regenerative braking strategy for electric vehicles," *Energies*, vol. 4, no. 9, pp. 1461–1477, Sep. 2011.
[21] M. J. Yang, H. L. Jhou, B. Y. Ma, and K. K. Shyu, "A cost-effective method of electric brake with energy regeneration for electric vehicles," *IEEE Trans. Ind. Electron.*, vol. 56, no. 6, pp. 2203–2212, Jun. 2009.
[22] F. Zhu, Z. Yang, Z. Zhao, and F. Lin, "Two-stage synthetic optimization of supercapacitor-based energy storage systems, traction power parameters and train operation in urban rail transit," *IEEE Trans. Veh. Technol.*, vol. 70, no. 9, pp. 8590–8605, Sep. 2021.
[23] M. U. Deepa and G. R. Bindu, "A novel switching scheme for regenerative braking and battery charging for BLDC motor drive used in electric vehicle," in *Proc. IEEE Int. Power Renew. Energy Conf.*, Oct. 2020, pp. 1–6.
[24] T. Soylu and R. Bayır, "Downhill speed control of in-wheel motor during regenerative braking," *Elektronika ir Elektrotechnika*, vol. 23, no. 6, pp. 40–45, Dec. 2017.
[25] S. Heydari, P. Fajri, M. Rasheduzzaman, and R. Sabzehgar, "Maximizing regenerative braking energy recovery of electric vehicles through dynamic low-speed cutoff point detection," *IEEE Trans. Transport. Electrific.*, vol. 5, no. 1, pp. 262–270, Mar. 2019.
[26] S. Heydari, P. Fajri, R. Sabzehgar, and A. Asrari, "Optimal brake allocation in electric vehicles for maximizing energy harvesting during braking," *IEEE Trans. Energy Convers.*, vol. 35, no. 4, pp. 1806–1814, Dec. 2020.
[27] A. J. Godfrey and V. Sankaranarayanan, "A new electric braking system with energy regeneration for a BLDC motor driven electric vehicle," *Int. J., Eng. Sci. Technol.*, vol. 21, no. 4, pp. 704–713, Aug. 2018.
[28] X. Nian, F. Peng, and H. Zhang, "Regenerative braking system of electric vehicle driven by brushless DC motor," *IEEE Trans. Ind. Electron.*, vol. 61, no. 10, pp. 5798–5808, Oct. 2014.
[29] X. Zhang, Y. Wang, G. Liu, and X. Yuan, "Robust regenerative charging control based on T–S fuzzy sliding-mode approach for advanced electric vehicle," *IEEE Trans. Transport. Electrific.*, vol. 2, no. 1, pp. 52–65, Mar. 2016.
[30] G. Xu, K. Xu, C. Zheng, X. Zhang, and T. Zahid, "Fully electrified regenerative braking control for deep energy recovery and maintaining safety of electric vehicles," *IEEE Trans. Veh. Technol.*, vol. 65, no. 3, pp. 1186–1198, Mar. 2016.
[31] J. W. Dixon, M. Ortuzar, and E. Wiechmann. (2002). *Regenerative Braking for an Electric Vehicle Using Ultracapacitors and a Buck-Boost Converter*. [Online]. Available: https://hrudnick.sitios.ing.uc.cl/paperspdf/dixon/42a.pdf
[32] J. Dixon, I. Nakashima, E. F. Arcos, and M. Ortuzar, "Electric vehicle using a combination of ultracapacitors and ZEBRA battery," *IEEE Trans. Ind. Electron.*, vol. 57, no. 3, pp. 943–949, Mar. 2010.
[33] M. Ortuzar, J. Moreno, and J. Dixon, "Ultracapacitor-based auxiliary energy system for an electric vehicle: Implementation and evaluation," *IEEE Trans. Ind. Electron.*, vol. 54, no. 4, pp. 2147–2156, Aug. 2007.
[34] J.-H. Lee, D.-Y. Jung, T.-K. Lee, Y.-R. Kim, and C.-Y. Won, "Regenerative current control method of bidirectional DC/DC converter for EV/HEV application," *J. Electr. Eng. Technol.*, vol. 8, no. 1, pp. 97–105, Jan. 2013.
[35] K. Suresh, C. Bharatiraja, N. Chellammal, M. Tariq, R. K. Chakrabortty, M. J. Ryan, and B. Alamri, "A multifunctional non-isolated dual input-dual output converter for electric vehicle applications," *IEEE Access*, vol. 9, pp. 64445–64460, 2021.
[36] F. Naseri, E. Farjah, and T. Ghanbari, "An efficient regenerative braking system based on battery/supercapacitor for electric, hybrid, and plug-in hybrid electric vehicles with BLDC motor," *IEEE Trans. Veh. Technol.*, vol. 66, no. 5, pp. 3724–3738, May 2016.
[37] S. Jung and J. Ko, "Study on regenerative energy recovery of electric vehicle through voltage control using switched capacitor," *IEEE Trans. Veh. Technol.*, vol. 70, no. 5, pp. 4324–4339, May 2021.
[38] W. Yeo, S. Jung, S. Kim, K. Park, and J. Ko, "A regenerative energy recovery system for electric vehicles charging a battery at a low speed," *Adv. Sci., Technol. Eng. Syst. J.*, vol. 5, no. 2, pp. 64–73, 2020.
[39] J. Cao and A. Emadi, "A new battery/ultracapacitor hybrid energy storage system for electric, hybrid, and plug-in hybrid electric vehicles," *IEEE Trans. Power Electron.*, vol. 27, no. 1, pp. 122–132, Jan. 2012.
[40] M. B. Camara, H. Gualous, F. Gustin, and A. Berthon, "Design and new control of DC/DC converters to share energy between supercapacitors and batteries in hybrid vehicles," *IEEE Trans. Veh. Technol.*, vol. 57, no. 5, pp. 2721–2735, Sep. 2008.
[41] A. K. Podder, O. Chakraborty, S. Islam, N. M. Kumar, and H. H. Alhelou, "Control strategies of different hybrid energy storage systems for electric vehicles applications," *IEEE Access*, vol. 9, pp. 51865–51895, 2021.
[42] R. W. Erickson and D. Maksimovic, *Fundamentals of Power Electronics*, 2nd ed. Cham, Switzerland: Springer, 2001.
[43] J. Larminie and J. Lowry, *Electric Vehicle Technology Explained*. Hoboken, NJ, USA: Wiley, Aug. 2012.

TAKO NAMA (Student Member, IEEE) received the B.E. degree in electrical engineering from the Lalbhai Dalpatbhai College of Engineering, Ahmedabad, India, in 2010, and the M.Tech. degree from the North Eastern Regional Institute of Science and Technology, Nirjuli, India, in 2013. She is currently pursuing the Ph.D. degree with the Department of Electronics and Electrical Engineering, IIT, Guwahati, India. Her research interests include electric vehicle, system design and control, electrical drives, intelligent vehicles, and power electronics and its application in renewable energy systems.

PROSENJIT MONDAL received the B.Tech. degree in electrical engineering from the West Bengal University of Technology, Kolkata, India, in 2009, and the M.E. degree in power engineering from Jadavpur University, Kolkata, in 2012, and the Ph.D. degree from the IIT Guwahati, Guwahati, India, in 2021. From 2012 to 2013, he was an Assistant Professor at the Department of Electronics and Electrical Engineering, National Institute of Science and Technology. His interests include power electronics, control of electric drives, and renewable energy.

PRAVEEN TRIPATHY (Member, IEEE) received the M.Tech. and Ph.D. degrees from IIT Kanpur, Kanpur, India, in 2006 and 2011, respectively, all in electrical engineering. He is currently an Associate Professor with the Department of Electronics and Electrical Engineering, IIT Guwahati, India. His research interests include monitoring and control, power system dynamics, power system operation and control, FACTS, distribution automation, wind energy systems, microgrids, and electric vehicles.

RAVINDRANATH ADDA (Member, IEEE) received the B.E. degree from Andhra University, Visakhapatnam, India, in 2007, and the M.Tech. and Ph.D. degrees from the IIT Kanpur, Kanpur, India, in 2009 and 2014, respectively, all in electrical engineering. He is currently an Assistant Professor with the Department of Electronics and Electrical Engineering, IIT Guwahati, Guwahati, India. His research interests include power electronics for dc distribution systems, power quality, pulse-width modulation control techniques of inverters, and digital control in power electronics.

ANUP KUMAR GOGOI was born in Assam, India, in 1953. He received the B.E. degree in electrical engineering from the Assam Engineering College, Gauhati University, in 1976, and the M.Tech. and Ph.D. degrees in electrical engineering from IIT Kanpur, Kanpur, India, in 1981 and 1991, respectively. He was a Professor with IIT Guwahati, Guwahati, Assam. His research interests include electric drives, electro magnetics, microwave engineering, RF circuits, and systems design.